Dynamic Light-Scattering Study of Suspensions of fd Virus. Application of a Theory of the Light-Scattering Spectrum of Weakly Bending Filaments†

Tadakazu Maeda and Satoru Fujime*

Mitsubishi-Kasei Institute of Life Sciences, Machida, Tokyo 194, Japan.
Received March 4, 1985

ABSTRACT: We have presented a theoretical formulation of the field correlation function, $G^1(\tau)$, of polarized light quasi-elastically scattered from a suspension of very long ($\gtrsim 1$ μm) and weakly bending filaments.[2-7] Our formulation includes the effect on $G^1(\tau)$ of anisotropy in translational diffusion, of the filament flexibility, and of the hydrodynamic interaction. In order to examine the applicability of our formulation, suspensions of fd virus (895-nm length and 9-nm diameter) were experimentally studied as a model system. The entire profiles and the first cumulants of intensity correlation functions for highly monodisperse preparations were compared with computed ones based on our formulation for parameter values appropriate to fd virus, and it was found that the flexibility parameter γL is close to 0.23 at the solvent condition of 150 mM KCl and 15 mM phosphate buffer (pH 7.0). As a cross reference for independent measurements, a statistical analysis of virus images on electron micrographs was made, and it was found that the flexibility parameter is again close to 0.23. The numerical method for computation of $G^1(\tau)$ and experimental results for fd virus will be given in detail, and both the usefulness and the weakness of our formulation will be discussed.

Introduction

We have been interested in the dynamics of very long ($\gtrsim 1$ μm) and semiflexible (or weakly bending) filaments in solution, such as muscle F-actin, bacterial flagella, filamentous viruses, muscle thin and thick filaments. The Brownian movement of these filaments in solution is a superposition of translational, rotational, and flexing motions. It should be noted that translation of a long rod is anisotropic in solution; the sideway diffusion coefficient D_1 is smaller than the lengthway diffusion coefficient D_3. Then, the translational diffusion of the rod is no longer independent of the rotational diffusion.

On the basis of the Harris and Hearst model of polymer dynamics,[1] we have presented a theory of dynamic light-scattering spectrum of these filaments.[2-7] The latest formulation includes the anisotropy in translational diffusion, filament flexibility, and the effect of hydrodynamic interaction.[7] We are now able to compute the field correlation function $G^1(\tau)$ of polarized light scattered from a suspension of long and semiflexible filaments for given values of such model parameters as the filament length L, diameter d, transport coefficients D_1, D_3, and Θ (the rotational diffusion coefficient), and the inverse of the statistical length γ. When experimental values of L, d, D_1, D_3, and Θ are available, the only adjustable parameter is γ.

Tobacco mosaic virus is 300 nm in length and 18 nm in diameter and is considered to be a good model substance for a rigid rod. The dynamic light-scattering spectra for suspensions of tobacco mosaic virus were compared with those numerically computed with the model parameters appropriate to it.[8] The anisotropy in translational diffusion was found to be almost as large as that predicted from hydrodynamic theories of a rod friction factor.[9,10] As far as rigid rods are concerned, our formulation succeeded in predicting not only the initial decay rates of correlation functions but also their entire profiles.[8]

It is therefore timely for us to examine experimentally our formulation for a weakly bending filaments. The fd virus is 895 nm in length and 9 nm in diameter.[11] Its images under an electron microscope are slightly but nonuniformly curved. The fd virus seems to be a good model substance of a weakly bending filament for an examination of our theoretical model.

In this paper, we will at first review briefly our model of the dynamic light-scattering spectrum from dilute suspensions of very long and weakly bending filaments and give a numerical method to compute $G^1(\tau)$'s for model parameters appropriate to fd virus, where the value of γL is the only unknown and adjustable parameter. Second, we will estimate, as a cross reference, the virus flexibility from a statistical analysis of electron microscopic images of the virus. Third, the profiles and the initial decay rates of experimental intensity correlation functions will be compared with those of numerically computed correlation functions for various values of γL. Finally, we will discuss the usefulness and weakness of our formulation.

Theoretical Background

Let us denote the filament conformation by a space curve $\mathbf{r}(s,t)$, where s is the coordinate of a line element ds measured along the filament having length L ($-L/2 \leq s \leq L/2$) and t is time. We assume that the elastic potential energy of the filament is given by

$$V = (\epsilon/2)\int_{-L/2}^{L/2}[\partial^2\mathbf{r}(s,t)/\partial s^2]^2\,\mathrm{d}s \qquad (1)$$

where ϵ is a suitably defined elastic constant of the filament and is related to the parameter γ by $\epsilon = k_BT/(2\gamma)$.[6,7] Then, we have an operator that describes the free-draining force per unit length as $A(s) = \epsilon(\partial^4/\partial s^4)$, where we ignored the κ term in the Harris and Hearst model for $\gamma L \leq 0.5$. Eigenvalues λ_m and eigenfunctions $Q(m,s)$ of the operator $A(s)$ with free-end boundary conditions have been given in ref 6. In order to take account of the hydrodynamic interaction, we followed the method of Hearst, Beals, and Harris.[12] The spherically averaged interaction tensor has been introduced as[13]

$$H(s,s') = \delta(s - s') + (\zeta/6\pi\eta)f(|s - s'|)$$

where ζ is the friction factor per unit length and is set to $3\pi\eta$ throughout. An explicit form of $f(|s - s'|)$ will be found in ref 13. By the use of perturbation technique, we have

† Dedicated to Professor F. Oosawa on the occasion of his retirement from Osaka and Nagoya Universities. As early as 1967, he suggested to one of us (S.F.) the feasibility of detecting flexion modes of long and semiflexible scatterers by dynamic light scattering.

0024-9297/85/2218-2430$01.50/0

Table I
Hydrodynamic Interaction Factor f_m for fd Virus Particles[a]

m	f_m	m	f_m
2	2.453	6	1.640
3	2.208	7	1.502
4	1.987	8	1.380
5	1.800		

[a] Values of model parameters were L = 895 nm, d = 9 nm, and γL = 0.1. Although we computed f_m's for each γL values, the values in the table could be used for $0 < \gamma L \leq 0.5$ because of very little γL dependence of f_m.[7]

eigenvalues σ_m and eigenfunctions $\Psi(m,s)$ of the operator $\int H(s,s')A(s')[\text{operand}]\, ds'$ as[7]

$$\sigma_m = \lambda_m(1 + f_m)$$

$$\Psi(m,s) = \sum_j a_j(m)Q(m,s)$$

where f_m is the hydrodynamic interaction factor

$$f_m = (1/2)\int\int_{-L/2}^{L/2} Q(m,s)f(|s - s'|)Q(m,s')\, ds\, ds'$$

of which values for dimensions of fd virus are given in Table I. By normal mode expansion, we have $\mathbf{r}(s,t) = \sum_m \mathbf{q}(m,t)\Psi(m,s)$. Since the two lowest ($m$ = 0 and 1) of the normal modes correspond to the translational and rotational modes of the rod, respectively, we have $\mathbf{r}(s,t) = \mathbf{R}(t) + s\mathbf{t}(t) + \sum_m{}''\mathbf{q}(m,t)\Psi(m,s)$,[6] where $\mathbf{R}(t)$ and $\mathbf{t}(t)$ are the position and the orientation vectors of the rod at time t, respectively. Since these two modes couple with each other, we have to solve a coupled diffusion equation for translation and rotation in order to obtain the conditional probability $G(\mathbf{R}-\mathbf{R}',\mathbf{t},\mathbf{t}';\tau)$ that if a rod is found at $\mathbf{R}'$ with orientation $\mathbf{t}'$ at time t', it will be found at $\mathbf{R}$ with orientation $\mathbf{t}$ at a later time t ($\tau = |t - t'|$), which satisfies[5]

$$[\partial/\partial\tau - D_3(\mathbf{t}\cdot\partial/\partial\mathbf{R})^2 - D_1\{\partial^2/\partial R^2 - (\mathbf{t}\cdot\partial/\partial\mathbf{R})^2\} - \Theta\nabla_{\theta\phi}{}^2]G(\mathbf{R}-\mathbf{R}',\mathbf{t},\mathbf{t}';\tau) = \delta(\mathbf{R}-\mathbf{R}')\delta(\mathbf{t}-\mathbf{t}')\delta(\tau) \quad (2)$$

Since we are considering polarized scattered light, the ϕ dependence of G is not required. Let $G_K(\xi,\xi';\tau)$ be the Fourier space transform of G, where $\xi = \cos\theta$, θ being the angle between $\mathbf{t}$ and $\mathbf{K}$ (the scattering vector $\mathbf{K}$ being parallel to the laboratory-fixed polar axis), and define $G_K(\xi,\xi';\tau) = G_D(\tau)g_K(\xi,\xi';\tau)$, where $D_0 = (2D_1 + D_3)/3$ is the overall diffusion coefficient and

$$G_D(\tau) \equiv \exp[-\{D_0 - (1/3)(D_3 - D_1)\}K^2\tau] = \exp(-D_1K^2\tau) \quad (3)$$

An explicit form of $g_K(\xi,\xi';\tau)$ has been given in ref 5.

For the flexing motion of a filament, we have to solve the time-dependent part of the Langevin equation of motion for $\mathbf{q}(m,t)$ ($m \geq 2$).[6,7] Our previous method gives[7]

$$\langle\mathbf{q}(m,t)\cdot\mathbf{q}(m',t')\rangle = \langle\mathbf{q}(m,t)^2\rangle \exp(-\tau/\tau_m)\delta_{m,m'}$$

$$\langle\mathbf{q}_m{}^2\rangle \equiv \langle\mathbf{q}(m,t)^2\rangle \simeq 2k_BT/\lambda_m \quad \text{(with 99\% accuracy)}$$

$$\tau_m = \zeta_1/\sigma_m \qquad (\zeta_1 = 4\pi\eta)$$

We consider a dilute solution of weakly bending filaments and assume that the coupled translational/rotational diffusion of the filament is statistically independent of the flexing motion of the filament. Then, we have an expression for $G^1(\tau)$ as

$$G^1(\tau) = G_D(\tau)(1/L^2)\int\int_{-L/2}^{L/2} J(s,s',\tau)\, ds\, ds' \quad (4)$$

$$J(s,s',\tau) = (1/2)\int\int_{-1}^{1} d\xi\, d\xi' \, g_K(\xi,\xi';\tau)e^{iK(s\xi-s'\xi')}\prod_m{}''\exp[-\Phi(m,s,s',\xi,\xi',\tau)] \quad (5)$$

An explicit form of $\Phi(m,s,s',\xi,\xi',\tau)$ has been given in ref 6. Numerical studies showed that the four-fold integration in eq 4 and 5 can be approximated by three-fold integration with high accuracy provided that $\Phi(m,s,s',\xi,\xi',\tau)$ is replaced with $\Phi(m,s,s',\xi,\xi'=\xi,\tau)$.[6] Adopting this approximation, we arrive at the following expression for $J(s,s',\tau)$ (see eq 65 in ref 6):

$$J(s,s',\tau) = (1/2)\int_{-1}^{1} d\xi \prod_m{}''\exp[-(1 - \xi^2)\Phi_0(m,s,s',\tau)]\sum_n\sum_l (2l + 1)(-i)^l\mathbf{W}_{nl}(\tau)j_l(Ks')P_n(\xi)e^{iKs\xi} \quad (6)$$

where

$$\Phi_0(m,s,s',\tau) = (K^2/4)\langle\mathbf{q}_m{}^2\rangle \times [Q(m,s)^2 + Q(m,s')^2 - 2Q(m,s)Q(m,s')\exp(-\tau/\tau_m)] \quad (7)$$

$$\mathbf{W}_{nl}(\tau) = [\mathbf{U}\exp(-\Lambda^e\Theta\tau)\mathbf{U}^{-1}]_{nl} \quad \text{(even } n \text{ and } l\text{)}$$

$$\mathbf{W}_{nl}(\tau) = [\mathbf{V}\exp(-\Lambda^o\Theta\tau)\mathbf{V}^{-1}]_{nl} \quad \text{(odd } n \text{ and } l\text{)}$$

$$\mathbf{W}_{nl}(\tau) = 0 \quad \text{(mixed } n \text{ and } l\text{)}$$

Use of $Q(m,s)$ instead of $\Psi(m,s)$ in eq 7 is valid with very high accuracy even in the non-free-draining limit.[7] The matrices $\mathbf{U}$ and $\mathbf{V}$ are respectively the eigenvector matrices of the real tridiagonal matrices $\mathbf{M}^e$ and $\mathbf{M}^o$ derived from the coupled translational/rotational diffusion equation (explicit forms of $\mathbf{M}^e$ and $\mathbf{M}^o$ has been given in ref 6). The matrices Λ^e and Λ^o are the eigenvalue matrices of $\mathbf{M}^e$ and $\mathbf{M}^o$, respectively; i.e., $\mathbf{M}^e\mathbf{U} = \mathbf{U}\Lambda^e$ and $\mathbf{M}^o\mathbf{V} = \mathbf{V}\Lambda^o$. The functions $j_n(z)$ and $P_n(z)$ are respectively the nth-order spherical Bessel function and the nth-order Legendre polynomial. From the parity consideration, the integral region could be reduced to one-eighth of the original (see Appendix).

Numerical Method

We computed $G^1(\tau)$ on a 16 bits/word minicomputer (Nippon Data General, Eclipse S140) running under a mapped real-time disk operating system (MRDOS, Revision 7.0). The machine was equipped with 256-kbyte memory, a memory management and protection unit (MMPU), and a floating-point unit (FPU). The time required to compute a value of $G^1(\tau)$ for a specific value of τ was about 10 min on our minicomputer, of which performance was 0.45 MWIPS (mega Whetstone instructions per second) for single-precision floating-point arithmetic. Computation time for $G^1(\tau)$ will be shortened on a larger computer. Figure 1 shows the flow chart of our program, which was written in Fortran 5 (Data General's dialect of Fortran IV), and fully took advantage of overlays and virtual arrays to circumvent the limitation of the addressing range of our minicomputer (=64 kbytes). Subroutines used in our computation have been more or less specifically tailored to clear the above limitation and for speed consideration. Following are the major subroutines we used: CADRE[14] and ADAPT,[15] which are adpative quadrature subroutines in one and multidimensions, respectively, were partially modified to use virtual arrays for their stacking area. FIGI2 and IMTQL2,[16] which compute all eigenvalues and eigenvectors of a special real tridiagonal matrix, were also modified to use virtual arrays for their working area. JSBES,[17] a subroutine that outputs a value of $j_n(z)$ for the input arguments of n and z, was partially

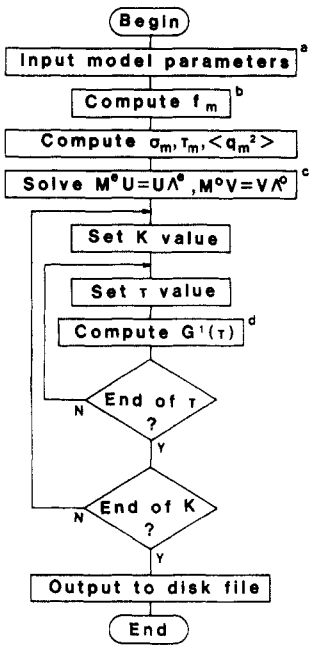

Figure 1. Flow chart of the numerical computation of $G^1(\tau)$. Notes and comments: (a) model parameters are L, d, D_1, D_3, Θ, and γ; (b) since integration over s' can be carried out analytically,[7] the subroutine CADRE was used at this step; (c) to solve matrix eigenvalue problems, subroutines IMTQL2 and FIGI2 were used; (d) to compute $G^1(\tau)$ by use of eq A2, the subroutine ADAPT was used and to compute the integrand of eq A2, subroutines JSBES and LEP were used.

modified to output all values of $j_m(z)$ for $m = 0, 1, 2, ..., n$ at the return of the subroutine. LEP,[17] a subroutine that outputs all values of $P_m(z)$ for $m = 0, 1, 2, ..., n$ for the input arguments of n and z, was used without any modification.

We determined values of the computational and model parameters as follows.

(1) The size of the matrices $\mathbf{M}^e$ and $\mathbf{M}^o$: Let N' be the smallest number for which $(2N' + 1)b_{N'}(k)^2 \leq 10^{-6}G^1(0)$, where $b_n(k)$ is given in eq A4 in the Appendix. Then, the size of the matrices was determined by a relationship[5]

$$M_N = \min [2 \max (7, N', 2^{1/2}\mu), 61]$$

(2) Number of bending modes and range of K^2: The internal modes in eq A1 (or eq 7) were taken up to $m = 8$.[4] The range of K^2 was from 0.5 to 12 in units of 10^{10} cm^{-2}, which covers the experimentally accessible range for a 488-nm beam from an Ar^+ laser.

(3) Model parameters: The hydrodynamic properties of fd virus have been extensively studied.[11] Reported values of the hydrodynamic parameters are $L = (895 \pm 20)$ nm, $d = (9 \pm 1)$ nm, $D_0 = (2.58 \pm 0.04) \times 10^{-8}$ cm^2/s at 25 °C and $\Theta = (20.9 \pm 0.3)$ s^{-1} at 20 °C (both at the concentration [fd] $\rightarrow$ 0). The above values of L and d were determined in ref 11 by use of Broersma's formulas[9,11] for a *rigid* rod; for $L_p = \ln(2p)$ and $p = L/d$, they are expressed as

$$D_0 = (k_B T/3\pi\eta L)[L_p - \tfrac{1}{2}(\delta_1 + \delta_3)]$$

$$\Theta = (3k_B T/\pi\eta L^3)(L_p - \delta_\theta)$$

$$\delta_1 = 0.19 - 4.2(1/L_p - 0.39)^2$$

$$\delta_3 = 1.27 - 7.4(1/L_p - 0.34)^2$$

$$\delta_\theta = 1.45 - 7.5(1/L_p - 0.27)^2$$

Since fd virus is only slightly flexible, we have[18,19]

$$D_0(\text{semiflexible}) = D_0(\text{rigid}) f_{t,0}(L,d,\gamma L)$$

$$\Theta(\text{semiflexible}) = \Theta(\text{rigid}) f_r(L,d,\gamma L)$$

For $L/d = 100$ and $\gamma L = 0.2$, for example, we have $f_r = 1.105$[19a] and 1.116[19b] (and $f_{t,0} \simeq f_r^{1/3} = 1.03$–1.04). These values of f_r suggest that L of fd virus may be 3–4% longer than the above value of $L = 895$ nm (an effect of slightly different L values on $G^1(\tau)$ will be discussed later). Since, however, a correction factor $f_{t,1}$ for D_1 is expected to be very close to $f_{t,3}$ for D_3, we will have $D_1(\text{semiflexible})/D_3(\text{semiflexible}) = D_1/D_3$, where Broersma's formulas give

$$D_1 = (k_B T/4\pi\eta L)(L_p - \delta_1)$$

$$D_3 = (k_B T/2\pi\eta L)(L_p - \delta_3)$$

From $D_0(\text{observed}) = [2D_1(\text{semiflexible}) + D_3(\text{semiflexible})]/3$ and the above relations, we could obtain $D_1(\text{semiflexible}) \equiv D_0(\text{observed})(D_1/D_0) = 1.19$ and $D_3(\text{semiflexible}) \equiv D_0(\text{observed})(D_3/D_0) = 1.88$ in units of 10^{-8} cm^2/s at 5 °C. [The factors $L_p - \delta_j$ of Broersma's expressions[9] are a little different from those of de la Torre's expressions;[10] $D_1/D_3 = 0.6286$[9] and 0.6177,[10] or $D_1(\text{semiflexible}) = 1.17$ and $D_3(\text{semiflexible}) = 1.90$ in units of 10^{-8} cm^2/s for de la Torre's values.] The friction factor $\zeta_1 = 4\pi\eta$ in $\tau_m = \zeta_1/\sigma_m$ was equally determined by the relationships[7]

$$\tau_m = (\pi^4/24\gamma L)(m - \tfrac{1}{2})^4(12D_1^\circ/L^2)(1 + f_m) = (\pi^4/24\gamma L)(m - \tfrac{1}{2})^4\Theta^\circ(1 + f_m)$$

where $D_1^\circ \equiv D_1(\text{semiflexible})/(1 + f_0)$ and $\Theta^\circ \equiv \Theta(\text{observed})/(1 + f_1)$. The reason the tabulated η value was not used to evaluate $\zeta_1 = 4\pi\eta$ came from a consideration that the factor $(D_1/L^2)(1 + f_m)/(1 + f_0)$ or $\Theta(1 + f_m)/(1 + f_1)$ will be less sensitive to both a little ambiguity in the L value (due to a slight filament flexibility) and the approximation we assumed in formulating f_m. The flexibility parameter γL was treated as an adjustable parameter, which was varied in a range 0.0–0.5. When the flexibility parameter is independent of temperature, the correlation function can scale with T/η.[20] Since experimental correlation functions for dilute suspensions of fd virus have been known to scale with T/η,[21] all computations of $G^1(\tau)$ were carried out for parameter values at the temperature of measurements. After the analysis of computed correlation functions, the results were corrected to 5 °C.

We computed $G^1(\tau)$ at delay times of 0 s and 1 μs to 0.5 s in steps of 1, 2, and 5 within 0.1% relative errors. PCUBIC and SPLINE[22] recovered and approximated the value of $G^1(\tau)$ at an arbitrary value of $\tau \leq 0.5$ s from a table of ln $[G^1(\tau)]$ computed as above. The theoretical intensity correlation function $Y_c(\tau)$ was constructed and analyzed as follows: First, we determined τ_{max} so that it satisfies $G^1(\tau_{max})/G^1(0) = 0.3$ or 0.1 and computed $Y_c(\tau) \equiv [G^1(\tau)/G^1(0)]^2 + 1$ for $\tau = n(\tau_{max}/128)$ with $n = 1, 2, ..., 128$. $Y_c(\tau)$ was analyzed with the *same* program as was used in analyzing experimental correlation functions. It was found that at intermediate and larger K^2 values, the first cumulant $\bar{\Gamma}$ of $Y_c(\tau)$'s for the above two τ_{max} values differed appreciably. This was due to stronger contributions of internal modes to $G^1(\tau)$. To avoid ambiguity in theoretical $\bar{\Gamma}$ values coming from different τ_{max} values, we finally decided to prepare $Y_c(\tau)$ for $\tau_{max}/128$ equal to the channel width at the measurement. As far as the comparison of $\bar{\Gamma}$ values is concerned, the last method is free from the choice of the channel width at the measurements.

Materials and Methods

1. **Medium and Buffer.** A trypton medium contained (per liter) 10 g of bactotrypton (DIFCO), 1 g of yeast extract (DIFCO), 8 g of NaCl, 1 g of glucose, 0.5 g of tris(hydroxymethyl)aminomethane, and 5 mL of sterile 1 M $CaCl_2$ added after autoclaving. A standard buffer solution contained 150 mM KCl and 15 mM

phosphate buffer (pH 7.0) and was cleaned with a 0.1-μm-pore membrane filter just before use.

2. Preparation of fd Virus. Wild type fd virus was grown on *Escherichia coli* strain S-26 cultured in the trypton medium. Purification procedures, carried out at 4 °C, included two cycles of polyethylene glycol phase separation[23] followed by equilibrium banding in CsCl density gradients and dialysis against the standard buffer solution. We had to be very careful not to give unnecessary shear force to the virus suspension during the process of preparation. Otherwise, virus particles shorter than native ones appeared.

3. Concentration Measurement. Concentrations of virus were determined by UV absorbance measurements done on a Cary 17 double-beam recording spectrophotometer by adopting the value of optical density at 269 nm to be 3.84 for a 1 mg/mL virus suspension and a 1-cm optical path length.[24]

4. Electron Microscopy. The fd virus particles were spread on carbon-coated microgrids treated with an ion coater (Eiko, Type IB-3) and negatively stained with 4% uranyl acetate. In a conventional spread method, we touched a specimen grid to a drop of virus suspension and removed the excess solution on the grid with a piece of filter paper. Electron micrographs obtained with this method had a very uniform background, and images of fd virus were clearly seen from one end to the other. Virus particles left on the grid, however, were more or less oriented by flow occurring on removal of the excess solution from the grid. Thus, this method was adopted when length distribution of virus was examined. In a microdroplet method,[25] a cytochrome *c* monolayer was first formed on a surface of a drop of the sample solution containing both fd virus and cytochrome *c* and virus particles in the drop spontaneously adsorbed on the monolayer within several to several tens of minutes. Then, we touched a specimen grid face down to the surface of the drop, washed with doubly distilled water, and removed the excess water with a piece of filter paper. The electron micrographs obtained with this method had rather granular backgrounds, and the ends of the individual virus were a little unclear compared with those with the former method. Since, however, it is no matter (see paragraph 5 below) and the virus particles observed with this method were the ones spontaneously stuck to the cytochrome *c* monlayer, their shape would be worthy of being statistically analyzed for the estimation of the virus flexibility.

The specimen grids were observed under a JEOL 100B electron microscope operating at 60–80 kV with a nominal magnification of 15 000 without absolute calibration. For measurements of contour lengths L and the end-to-end distance R of fd virus, images of the fd virus on electron micrographs were projected onto a graphic digitizer (Kontron Messgerade Co., FRG, Type AM-02). The total magnification of the virus images was 60 000–100 000 on the digitizer. It was possible to measure lengths of images within 0.1 mm on the digitizer.

5. Statistical Analysis of Images of fd Virus. For an image of a filament "frozen" on a two-dimensional substrate, we have[26]

$$\langle R^2\rangle/L^2 = f_2(\gamma,L) = 2[\exp(-\gamma L) - 1 + \gamma L]/(\gamma L)^2 \quad (8)$$

where $\langle R^2\rangle$ is the mean-square end-to-end distance of the filament. Equation 8 has been derived from the basic assumption of eq 1, and it is a two-dimensional version of $\langle R^2\rangle/L^2 = f_3(\gamma,L) = 2[\exp(-2\gamma L) - 1 + 2\gamma L]/(2\gamma L)^2$ in three dimensions. The most probable γ value can be determined by minimizing the sum over all filaments j of $[R_j/L_j - f_2(\gamma,L_j)^{1/2}]^2$ with respect to γ. Details of the procedure will be found in ref 27. For a highly monodisperse preparation as in our case (see Figure 3), the $\gamma\bar{L}$ value will be the most probable γL value independent of total magnification of the filament image, where $\bar{L}$ is the mean of L_j's. Since eq 8 holds, in principle, for L_j and R_j between *any* two points on a filament and since our graphic digitizer computes R_j from the (x,y) coordinates of the initial and final points for the measurement of L_j, a little vague appearance of the ends of the filament images on micrographs does not affect an accuracy in the estimation of γL.

6. Preparation of Scattering Samples. Virus suspensions were centrifuged at 40000*g* for 1 h. A known volume of the supernatant was diluted in a scattering cell to a desired concentration with a standard buffer solution. The suspension in the scattering cell was centrifuged at 3000*g* for 1–48 h and used for the dyamic light-scattering measurements.

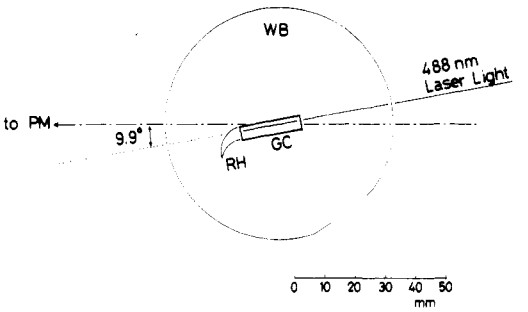

Figure 2. Top view of a low-angle scattering geometry; (WB) a water bath; (GC) a rectangular glass cell of 30 (height) × 4 (width) × 20 (length) mm³; (RH) a Rayleigh horn; (PM) a photomultiplier tube.

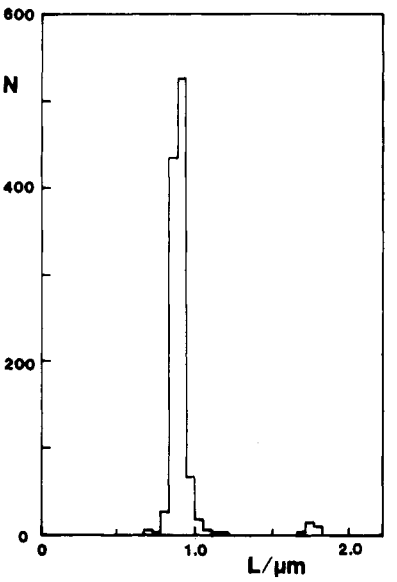

Figure 3. Length distribution of fd virus particles for a total number of 1130.

7. Dynamic Light-Scattering Measurements. An optical system for scattering angles of 30–150° and a method of data collection have been described elsewhere.[28] A system for a low angle was additionally set up, where a rectangular glass cell of dimensions 20 × 4 × 30 mm³ was immersed in a water bath (Figure 2). The geometrical scattering angle was 9.9°, but the true scattering angle was 10.3° after correction of refractive index difference between water and buffer. Refractive index of the buffer solution was measured with an Abbe refractometer (Atago Inc.). All the measurements were done at 24–25 °C (measured within ± 0.05 °C before and after each measurement of correlation functions). The light source was a 488-nm beam from an Ar^+ laser (Lexel, Model 95).

A homemade 128-channel, single-clipped digital correlator was used, which was interfaced to a minicomputer (Nippon Data General, Nova 02-30).[28]

8. Analysis of Correlation Functions. Experimental intensity correlation functions were analyzed with a cumulant expansion method[29] up to the third order. A linearized expansion formula was found not to be very good for correlation functions $Y_m(\tau)$ at intermediate and larger K^2 values. So, we adopted

$$Y_m(\tau) - B = \beta[\exp(-\bar{\Gamma}\tau)\{1 - (\mu_2/2)\tau^2 + (\mu_3/6)\tau^3\}]^2$$

where B is the base-line level. The first cumulant $\bar{\Gamma}$ was corrected to 5 °C.

Results and Discussion

Length Distribution of fd Virus. Figure 3 shows an example of the length distribution of fd virus. A slight amount of double-length particles was observed, but the number ratio of double-length to single-length particles

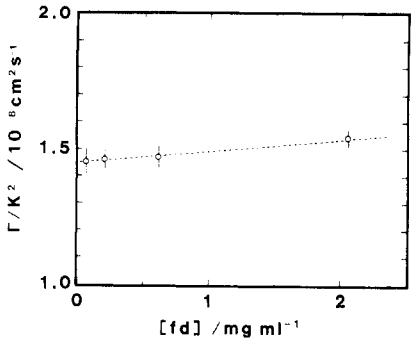

Figure 4. $\bar{\Gamma}/K^2$ vs. [fd] relationship at the scattering angle of 10.3°. The $\bar{\Gamma}/K^2$ values were scaled to 5 °C. The solvent was 150 mM KCl and 15 mM phosphate buffer (pH 7.0).

was less than 3%. Our preparation was highly monodisperse.

Statistical Analysis of Virus Images. Contour lengths and end-to-end distances of about 900 images of fd virus particles were analyzed by use of eq 8, and the flexibility parameter was determined to be $\gamma L = 0.225 \pm 0.027$. Because of possible artifacts introduced in the sample preparation for electron microscopy, this value may not have the absolute meaning its digits give, but $\gamma L \simeq 0.23$ will be an estimate of the flexibility parameter of fd virus.

Translational Diffusion Coefficient of fd Virus. Figure 4 shows the $\bar{\Gamma}/K^2$ vs. [fd] relationship at the scattering angle of 10.3° ($K^2 = 9.47 \times 10^8$ cm^{-2}), from which we have a value of $\bar{\Gamma}/K^2$ at [fd] = 0 of 1.45×10^{-8} cm^2/s. At this scattering angle, the filament flexibility contributes little to the $\bar{\Gamma}$ value, whereas the rotational Brownian motion may. For a rod whose axial ratio is 100, Broersma's formulas give $D_3 - D_1 \simeq 0.5D_0$. The apparent diffusion coefficient $\bar{\Gamma}/K^2$ for a rigid rod depends on $k = KL/2$ as[5]

$$\bar{\Gamma}/K^2 = D_0 + (L^2/12)\Theta f_1(k) - (D_3 - D_1)[1/3 - f_2(k)]$$

where both $f_1(k)$ and $f_2(k)$ are functions depending only on k and their values are tabulated in ref 5. At $K^2 = 9.47 \times 10^8$ cm^{-2}, we have $f_1 = 0.090$ and $^1/_3 - f_2 = 0.056$. From the values of $\Theta = 13.1$ s^{-1}, $L = 895$ nm, $D_3 - D_1 = 0.5D_0$ and $\bar{\Gamma}/K^2 = 1.45 \times 10^{-8}$ cm^2/s, we have $D_0 = 1.41 \times 10^{-8}$ cm^2/s at 5 °C. This value agrees with the D_0 value reported in ref 11, $D_0 = 2.58 \times 10^{-8}$ cm^2/s at 25 °C or 1.41×10^{-8} cm^2/s at 5 °C. This will ensure our use of the Θ value in ref 11 for our analysis. [It should be mentioned that for the vertically polarized incident beam, the ratio of horizontally to vertically polarized scattering, I_h/I_v, was 0.3% for 0.06 mg/mL and 0.5% for 2 mg/mL virus suspensions.]

Correlation Function Profiles. Figure 5 shows profiles of computed and experimental $|g^1(\tau)|^2$ at the scattering angles of 45° ($K^2 = 1.718 \times 10^{10}$ cm^{-2}) and 105° ($K^2 = 7.383 \times 10^{10}$ cm^{-2}). At both scattering angles, the effect of filament flexibility on entire profiles can be seen, and it is suggested that the γL value of fd virus is close to 0.2. This is more quantitatively examined below.

$\bar{\Gamma}/K^2$ vs. K^2 Relationships. Figure 6 shows the $\bar{\Gamma}/K^2$ vs. K^2 relationships of computed and experimental $|g^1(\tau)|^2$. From the molecular weight $M_r = 1.67 \times 10^7$[11] and $L = 895$ nm of the fd virus, we have a relationship $cL^3 = 26.2c_p$, where c is the number of particles in unit volume and c_p is the concentration of particles in units of mg/mL. Then [fd] = 0.088 mg/mL corresponds to $cL^3 = 2.3$, which is out of a dilute regime $cL^3 \ll 1$. According to transient electric birefringence measurements,[11,30] however, no sign of the onset of the semidilute region in the experimental Θ values of fd virus was observed up to almost $cL^3 = 5$. Thus, the

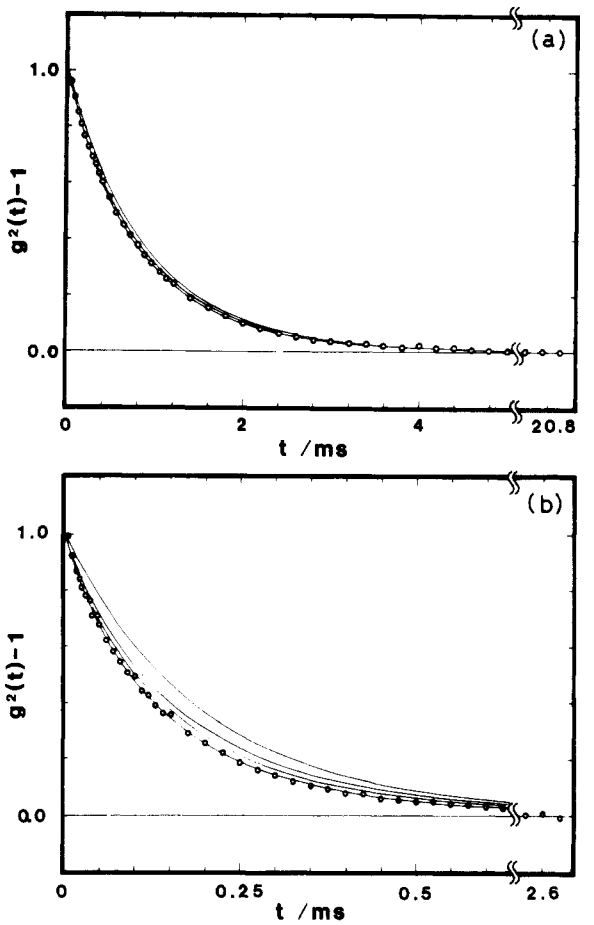

Figure 5. Profiles of computed (—) and experimental (○) correlation functions. To avoid the cluttering, every second point is displayed from the *11th* to the *30th* channel and every fifth point from the *31st* to the last channel. Temperature was 24.4 °C and [fd] = 0.088 mg/mL. Solvent was the same as in Figure 4. (a) At the scattering angle of 45°. The computed profiles from top to bottom are for $\gamma L = 0.0$, 0.1, and 0.2, respectively. (b) At the scattering angle of 105°. The computed profiles from top to bottom are for $\gamma L = 0.0$, 0.05, 0.1, and 0.2, respectively.

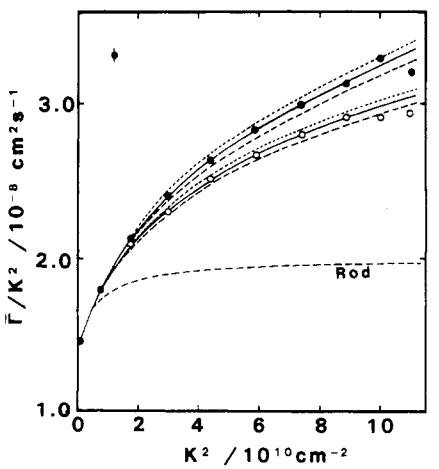

Figure 6. $\bar{\Gamma}/K^2$ vs. K^2 relationships of computed and experimental correlation functions. [fd] = 0.088 mg/mL and other conditions were the same as those in Figure 4. (○) The second-order and (●) the third-order nonlinear cumulant expansion. (– – –) $\gamma L = 0.20$, (—) $\gamma L = 0.23$, and (···) $\gamma L = 0.25$. To avoid cluttering, a typical size of the error bar is shown at a corner. [A linearized second-order analysis was made previously for $G^1(\tau_{max})/G^1(0) = 0.3$,[7] τ_{max} being defined in Numerical Method; see also (○) and (—) in Figure 7.]

experimental results in Figure 6 can be compared with the theoretical ones for a dilute regime. From the results in

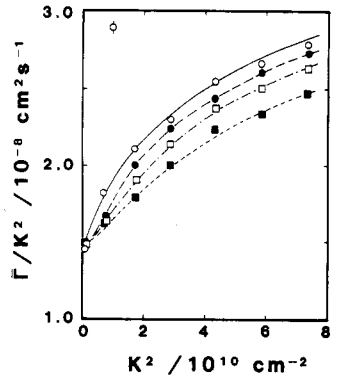

Figure 7. $\bar{\Gamma}/K^2$ vs. K^2 relationships for various [fd]. A linearized second-order expansion was applied. [fd] in units of mg/mL were 0.088 for (○), 0.27 for (●), 0.66 for (□), and 1.32 for (■). Other conditions were the same as those in Figure 4. To avoid cluttering, a typical size of the error bar is shown at a corner.

Figure 6, we can clearly see that the flexibility parameter of fd virus is very close to 0.23 (in both the second-order and the third-order analyses) in the present solvent condition. It is interesting to compare the γL value from dynamic light scattering with that from electron microscopy.

$\bar{\Gamma}/K^2$ vs. K^2 Relationships of Less Dilute Suspensions. Figure 7 shows the $\bar{\Gamma}/K^2$ vs. K^2 relationships when [fd] was changed. As [fd] was increased, the $\bar{\Gamma}/K^2$ values at $\theta = 10.3°$ slightly increased (Figure 4), whereas those at $\theta \geq 30°$ decreased. These features probably suggest that in less dilute suspensions, both translational and flexing motions of a virus particle are not very much restricted by surrounding particles, whereas its rotational motion is heavily restricted. As was discussed previously,[6,28] the translational and flexing motions will be almost free from restriction when the average interfilament spacing is larger than $1/K$ and the mean amplitude of filament flexing, respectively. On the other hand, the rotational motion will not be free from restriction when the average interfilament spacing is smaller than the filament length. Our formulation is based on eq 2 for the free translational and rotational Brownian motion of a rod. Therefore, it can not directly be applied to cases of less dilute suspensions. However, to the first-order approximation, a simple replacement of Θ with $\bar{\Theta}$ in our formulation may work, where $\bar{\Theta}$ is the rotational diffusion coefficient in less dilute suspensions. Doi and Edwards have given $\bar{\Theta}/\Theta = k(cL^3)^{-2}$, where k is a proportionality constant expected to be within an order of 10.[31] The restriction imposed by Doi and Edwards has been pointed out to be too strong (e.g., ref 28). The Monte Carlo simulation by Doi et al.[32] and a new formulation by Teraoka et al.[33] give a much better cL^3 dependence of $\bar{\Theta}$. From an experimental point of view, it is desirable to measure dynamic light-scattering spectra and transient electric birefringence relaxation spectra, for example, at the same experimental condition and to use $\bar{\Theta}$ values from the latter spectra to simulate the former spectra. From a theoretical point of view, we have to seek an equation of motion of a rod that is better than eq 2. The equation of motion should include not only steric but also other types of interparticle interactions. These are postponed until a future study.

The following facts should be mentioned. Contrary to the results of Maguire on the same fd virus,[34] the apparent diffusion coefficient $\bar{\Gamma}/K^2$ did not show a tendency to converge toward $D_3/3$, the semidilute limit of Doi and Edwards.[31] Also, our results did not show such long tails in correlation functions (Figure 8) as Maguire has reported.[34]

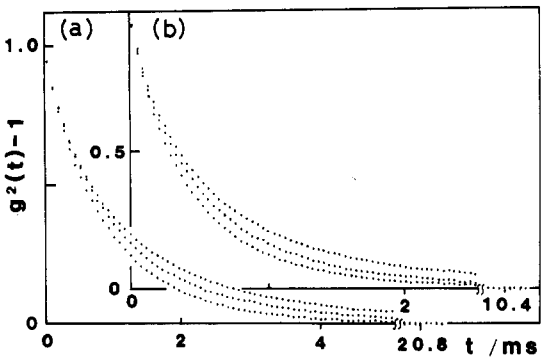

Figure 8. Correlation function profiles at different [fd]. From bottom to top, [fd] = 0.088 (cL^3 = 2.3), 1.32 (35), and 2.85 (75) in units of mg/mL, respectively. Temperature was 24.4 °C and the scattering angles were (a) 45° and (b) 60°. Solvent was the same as in Figure 4. In order to show the tail behavior of correlation functions, the value of the first channel was simply normalized to unity and the every second point is displayed from the second to the last channel.

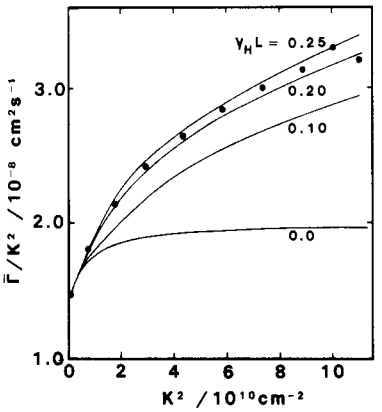

Figure 9. $\bar{\Gamma}/K^2$ vs. K^2 relationship of computed (—) and experimental (●) correlation functions. Computation was based on eq 9 (for the definition of γ_H, see text). A nonlinear third-order expansion was applied. Experimental points were from data for [fd] = 0.088 mg/mL (the same as (●) in Figure 6).

Supplemental Discussion. If we ignore anisotropy in translational diffusion; i.e., $D_3 = D_1$, we have $\mathbf{W}_{nl}(\tau) = \exp[-n(n+1)\Theta\tau]\delta_{nl}$. Then our old model (eq 7 in ref 4) gives

$$J^*(s,s',\tau) = \sum_n{}''(2n+1)\exp[-n(n+1)\Theta\tau]j_n(Ks)j_n(Ks')\prod_m{}''\exp[-\Phi_0^*(m,s,s',\tau)]$$

$$\Phi_0^*(m,s,s',\tau) = (K^2/6)\langle \mathbf{q}_m^2\rangle \times [Q(m,s)^2 + Q(m,s')^2 - 2Q(m,s)Q(m,s')\exp(-\tau/\tau_m)]$$

To take account of anisotropy in translation approximately, we introduce $G_D^*(\tau)$ instead of $G_D(\tau)$ in eq 3[6]

$$G_D^*(\tau) = \exp[-\{D_0 - \tfrac{1}{3}(D_3 - D_1)(1 - 3f_2(k))\}K^2\tau]$$

Then we have

$$G^1(\tau) = G_D^*(\tau)(1/L^2)\int\int_{-L/2}^{L/2} J^*(s,s',\tau)\,ds\,ds' \quad (9)$$

with $\epsilon = 3k_BT/(4\gamma_H)$. Computation of eq 9 is very much easier than that of eq 4. By taking non-free-draining values of τ_m, we computed eq 9 for parameter values for fd virus, and the results are shown in Figure 9. The agreement between $\gamma_H L$ = 0.20–0.25 in Figure 9 and γL = 0.23 in Figure 6 is only apparent. It is easily shown that $\langle \mathbf{q}_m^2\rangle/6 = {}^2/_3\gamma_H/\beta_m^4$ and $\tau_m^{-1} = (1+f_m)(k_BT/\zeta_1)\beta_m^4/[2({}^2/_3\gamma_H)]$ in Φ_0^* and $\langle \mathbf{q}_m^2\rangle/4 = \gamma/\beta_m^4$ and $\tau_m^{-1} = (1+f_m)(k_BT/$

$\zeta_1)\beta_m^4/(2\gamma)$ in eq 7, where $\beta_m = \pi(m - {}^1/_2)/L$. Equation 9 is the same as eq 69 in ref 6 for $\Delta = 1$ and $\gamma = {}^2/_3\gamma_H$, provided that $\exp(-DK^2\tau)$ in the latter equation is replaced with $G_D^*(\tau)$. Therefore, $\gamma_H L = 0.20$–0.25 corresponds to $\gamma L = 0.13$–0.17; the lower bound of the γL value of the fd virus. Nevertheless, if we regard γ_H estimated from eq 9 as γ in $\epsilon = k_B T/(2\gamma)$, eq 9 can be used to roughly estimate the flexural rigidity from high-angle data of very long and weakly bending filaments. More discussion will be found in ref 6.

Concluding Remarks

Since the adopted values of model parameters, L and d, in our computation of $G^1(\tau)$ have been determined from experimental values of D_0 (from low-angle dynamic light scattering) and Θ (from transient electric birefringence) by the aid of Broersma's formulas for D_0(rigid) and Θ(rigid),[11] all other model parameters, D_1, D_3, and τ_m, in our computation are said in effect to be determined by Broersma's formulas for *given values* of L and d. As mentioned in Numerical Method, a correction factor will arise; i.e., Θ(semiflexible) = Θ(rigid)$f_r(L,d,\gamma L)$, and the new L value may be 3–4% longer than the assumed value of 895 nm. This new L value is considered not to strongly affect the estimation of D_1, D_3, and τ_m as mentioned before (Numerical Method). The strongest effect of the L value will appear on Φ_0 in eq 7. Since $\langle \mathbf{q}_m{}^2 \rangle \propto (\gamma L)L^3$ and since one L in $\langle \mathbf{q}_m{}^2 \rangle$ cancels the normalization constant of $Q(m,s)$, Φ_0 is proportional to $(\gamma L)L^2$. The new L value increases the Φ_0 value by $(1.03$–$1.04)^2 = 1.06$–1.08. To compensate this increase, the γL value has to be decreased. Indeed, computation of $G^1(\tau)$'s for $L = 1.035 \times 895$ nm and $\gamma L = 0.2$ gave $\bar{\Gamma}/K^2$ values that were a few percent larger than those for $L = 895$ nm and $\gamma L = 0.2$. In addition to this fact, the theoretical values of D_0 and Θ for given values of L and d (and γL) are appreciably different from one theory to another, and we have no definite criterion for the reasonableness of individual values. The worst situation in estimating the γL value could occur if a few uncertainties in the transport coefficients propagated to the final result cumulatively in a bad direction. If we had $\bar{\Gamma}/K^2$ values at low scattering angles where the filament flexibility has little effect on spectra, we could examine, at least, a gross reasonableness of the adopted values by a relationship $\bar{\Gamma}/(D_0K^2) = 1 + (L^2/12)K^2[(1/90)L^2\Theta/D_0 - (4/45)(D_3 - D_1)/D_0] + \ldots$, which is the low-$k$ limit of the $\bar{\Gamma}/K^2$ vs. K^2 relationship. (Note that two terms in [...] have values of about 2:1.) Because of technical difficulties, however, we have not yet studied the suspensions of fd virus at very low scattering angles. Therefore, the γL value from dynamic light scattering may have some ambiguity. As a cross reference, the γL value from measurements of the static scattering intensity seems to be the most desirable. Because of technical difficulties at very low scattering angles, however, we estimated the γL value by a statistical analysis of electron microscopic images of the virus. Since it is very difficult to evaluate possible artifacts introduced in the sample preparation for electron microscopy, this γL value has to be accepted as also subject to some ambiguity. In spite of these facts, a fairly good closeness of these two γL values will be worth noting.

Strictly speaking, only L, d, and γL are the molecular parameters required for the computation of $G^1(\tau)$. In a practical sense, on the other hand, there are many parameters, and it is not easy at present to quantitatively analyze experimental data for a weakly bending filament. However, large deviations of experimental $\bar{\Gamma}/K^2$ values from the theoretical curve for $\gamma L = 0.0$ in Figure 6 could be reasonably explained only when the filament flexibility was taken into account, as we have done approximately.

The operator that describes the free-draining force per unit length in the Harris and Hearst model is given by[1]

$$A(s) = \epsilon(\partial^4/\partial s^4) - \kappa(\partial^2/\partial s^2)$$

According to Soda,[35] the true force operator $KL \gtrsim 15$, form

$$A(s) = \epsilon(\partial^4/\partial s^4) - \kappa[(\mathbf{e}\cdot\partial^2/\partial s^2)\mathbf{e} + (u - 1)\partial^2/\partial s^2]$$

where $u = |\partial \mathbf{r}/\partial s|$ and $\mathbf{e}$ is the unit vector pointing in the direction tangent to the chain at s. Since Soda's operator is nonlinear, we have no simple way to solve eigenvalue problems. To avoid this difficulty, we put $\kappa = 0$ for a weakly bending filament,[6,7] so that our formulation is for "elastic" rods with flexural rigidity ϵ. In addition to this, we adopted a preaveraged hydrodynamic interaction tensor.[7] Our formulation is approximate in this sense, but it provides a practical procedure to estimate the flexibility parameter of weakly bending filaments in dilute suspension. Our formulation, however, has to be improved so as to hold for semidilute suspensions of weakly bending filaments.

It is worth noting that our old model with a slight modification can be used to approximately estimate the flexibility parameter of long filaments. This comes from the fact that for $KL \gtrsim 15$, the contribution to $\bar{\Gamma}/K^2$ from the translational/rotational motion, almost attains the saturation value (see the curve for $\gamma L = 0.0$ at $K^2 \geq 2 \times 10^{10}$ cm^{-2} in Figures 6 and 9). Kubota et al. found a drastic increase of the $\bar{\Gamma}/K^2$ values for suspension of *Limulus* thick myofilaments when the solvent was changed from a relaxing to an activating one.[36] According to our analysis based on eq 9,[37] the $\bar{\Gamma}/K^2$ vs. K^2 relationship of this filament in the relaxing solution could be explained by assuming a reasonable value of γL ("reasonable" in a sense that it does not conflict with electron microscopic images of the filament), whereas that in the activating solution could not be explained in a similar manner, suggesting the onset of another mode of motion in the latter. The light-scattering value of the filament flexibility of this myofilament is very close to that from image analysis of this filament in solution under an optical microscope (personal communication from Fan, Dewey, and Chu). In this kind of estimation, our old model, eq 9, is very useful, because eq 9 can be computed very easily even with a desk-top microcomputer.[37]

Acknowledgment. We thank Dr. Haruki Nakamura of University of Tokyo for kindly providing us seeds of *E. coli* strain S-26 and wild type fd virus and Dr. Tadayoshi Shiba of this institute for patiently helping us in preparation of fd virus. The technical advice of Shunzo Kondo of this institute was very helpful in electron microscopy. We also thank Miss Michiho Takasaki for her assistance.

Appendix: Reduction of the Integration Region

Let us define (cf. eq 6 in the text)

$$U(s,s',\xi,\tau) = \prod_m{}''\exp[-(1 - \xi^2)\Phi_0(m,s,s',\tau)]$$

$$g_n{}^e(s',\xi,\tau) = \sum_{\text{even } l} (2l + 1)(-i)^l \mathbf{W}_{nl}(\tau) j_l(Ks') P_n(\xi)$$

$$g_n{}^o(s',\xi,\tau) = \sum_{\text{odd } l} (2l + 1)(-i)^{l+1} \mathbf{W}_{nl}(\tau) j_l(Ks') P_n(\xi)$$

Since $P_n(-\xi) = (-1)^n P_n(\xi)$, we have from eq 6

$$J(s,s',\tau) = \int_0^1 d\xi\, U(s,s',\xi,\tau) \times [\cos(Ks\xi) \sum_{\text{even } n} g_n{}^e(s',\xi,\tau) + \sin(Ks\xi) \sum_{\text{odd } n} g_n{}^o(s',\xi,\tau)] \quad \text{(A1)}$$

Since $j_n(-z) = (-1)^n j_n(z)$, the first term in [...] in eq A1 is even for both s and s', whereas the second term is odd for both s and s'. Let us define

$$U^e(s,s',\xi,\tau) = \tfrac{1}{2}[U(s,s',\xi,\tau) + U(s,-s',\xi,\tau)]$$

$$U^o(s,s',\xi,\tau) = \tfrac{1}{2}[U(s,s',\xi,\tau) - U(s,-s',\xi,\tau)]$$

Since $Q(m,-s) = (-1)^m Q(m,s)$ and hence $U(-s,-s',\xi,\tau) = U(s,s',\xi,\tau)$, U^e and U^o are even and odd for both s and s', respectively. Then, from eq 4 and A1, we have for a weakly bending rod

$$G^1(\tau) = G_D(\tau)(4/L^2)\int\int_0^{L/2} ds\, ds' \int_0^1 d\xi\, [U^e(s,s',\xi,\tau) \times \cos(Ks\xi) \sum_{\text{even } n} g_n{}^e(s',\xi,\tau) + U^o(s,s',\xi,\tau) \sin(Ks\xi) \sum_{\text{odd } n} g_n{}^o(s',\xi,\tau)] \quad \text{(A2)}$$

For a rigid rod, we have $\langle \mathbf{q}_m{}^2 \rangle = 0$ and hence $\Phi_0 = 0$. By use of

$$\tfrac{1}{2}\int_{-1}^{1} P_n(\xi) \exp(iKs\xi)\, d\xi = i^n j_n(Ks)$$

we have from eq 4 and 6

$$G^1(\tau) = G_D(\tau) \sum_{\text{even } n,l} \sum (2l+1)(i)^{n+l} \mathbf{W}_{nl}(\tau) b_n(k) b_l(k) \quad \text{(A3)}$$

where for $k = KL/2$

$$b_n(k) = (1/k)\int_0^k j_n(z)\, dz \qquad \text{(even } n\text{)}$$

$$b_n(k) = 0 \qquad \text{(odd } n\text{)} \quad \text{(A4)}$$

Equation A2 was used for $0.5 \geq \gamma L \geq 1 \times 10^{-3}$ and eq A3 for $1 \times 10^{-3} > \gamma L \geq 0$.

References and Notes

(1) Harris, R. A.; Hearst, J. E. *J. Chem. Phys.* **1966**, *44*, 2595.
(2) Fujime, S. *J. Phys. Soc. Jpn.* **1970**, *29*, 751.
(3) Fujime, S.; Maruyama, M. *Macromolecules* **1973**, *6*, 237.
(4) Maeda, T.; Fujime, S. *Macromolecules* **1981**, *14*, 809.
(5) Maeda, T.; Fujime, S. *Macromolecules* **1984**, *17*, 1157, where D_3 in eq 39a and $(2n-5)$ in eq B2 should read $D_3/3$ and $(2n+5)$, respectively.
(6) Maeda, T.; Fujime, S. *Macromolecules* **1984**, *17*, 2381.
(7) Fujime, S.; Maeda, T. *Macromolecules* **1985**, *18*, 191.
(8) Kubota, K.; Urabe, H.; Tominaga, Y.; Fujime, S. *Macromolecules* **1984**, *17*, 2096, where $Y_m(I)^2$ in eq 16 should read $[Y_m(I) - Y_c(I)]^2$. See also: Wilcoxon, J.; Schurr, J. M. *Biopolymers* **1983**, *22*, 849.
(9) Broersma, S. *J. Chem. Phys.* **1960**, *32*, 1626, 1632.
(10) Tirado, M.; Garcia de la Torre, J. *J. Chem. Phys.* **1979**, *71*, 2581.
(11) Newman, J.; Swinney, H. L.; Day, L. A. *J. Mol. Biol.* **1977**, *116*, 593.
(12) Hearst, J. E.; Beals, E.; Harris, R. A. *J. Chem. Phys.* **1968**, *48*, 5371.
(13) Hearst, J. E.; Stockmayer, W. H. *J. Chem. Phys.* **1962**, *37*, 1452.
(14) de Boor, C. In "Mathematical Software"; Rice, J. R., Ed.; Academic Press: New York, 1971; pp 417–449.
(15) Genz, A. C.; Malik, A. A. *J. Comp. Appl. Math.* **1980**, *6*, 259.
(16) Smith, B. T.; Boyle, J. M.; Dongarra, J. J.; Barbow, B. S.; Ikebe, Y.; Clema, C. V.; Molar, C. B. "Lecture Notes in Computer Science", 2nd ed.; Springer-Verlag: New York, Heidelberg, Berlin, 1967.
(17) JSBES and LEP are subroutines included in Nippon Data General's Scientific Subroutine Package.
(18) (a) For $f_{t,0}(L,d,\gamma L)$, see: Yamakawa, H.; Fujii, M. *Macromolecules* **1973**, *6*, 407. (b) No report is available for $f_{t,1}(L,d,\gamma L)$ and $f_{t,3}(L,d,\gamma L)$, but an approximate expression $(D_3 - D_1)/D_0 = (3/4)[1 - 0.5(\gamma L)^{1/4}]$ is found in: Schmidt, M.; Stockmayer, W. H. *Macromolecules* **1984**, *17*, 509.
(19) (a) For $f_r(L,d,\gamma L)$, see: Yoshizaki, T.; Yamakawa, H. *J. Chem. Phys.* **1984**, *81*, 982; (b) Hagerman, P. J.; Zimm, B. H. *Biopolymers* **1981**, *20*, 1481.
(20) Fujime, S.; Maeda, T. *Biophys. J.* **1982**, *38*, 213.
(21) Newman, J.; Carlson, F. D. *Biophys. J.* **1980**, *29*, 37.
(22) Conte, S. D.; de Boor, C. In "Elementary Numerical Analysis. An Algorithmic Approach", 3rd ed.; MaGraw-Hill: New York, Toronto, London, 1980.
(23) Yamamoto, K. R.; Alberts, B. M.; Benzinger, R.; Lawhorne, L.; Treiber, G. *Virology* **1970**, *40*, 734.
(24) Berkowitz, S. A.; Day, L. A. *J. Mol. Biol.* **1976**, *102*, 531.
(25) Lang, D.; Mitani, M. *Biopolymers* **1970**, *9*, 373.
(26) Sugi, M.; Fuke, M.; Wada, A. *Polym. J. (Tokyo)* **1970**, *1*, 457.
(27) Mizushima-Sugano, J.; Maeda T.; Miki-Noumura, T. *Biochim. Biophys. Acta* **1983**, *755*, 25
(28) Fujime, S.; Ishiwata, S.; Maeda, T. *Biophys. Chem.* **1984**, *20*, 1.
(29) Koppel, D. E. *J. Chem. Phys.* **1972**, *57*, 4814.
(30) Maguire, J. F.; McTague, J. P.; Rondelez, F. *Phys. Rev. Lett.* **1980**, *45*, 1981; **1981**, *47*, 148.
(31) Doi, M.; Edwards, S. F. *J. Chem. Soc., Faraday Trans. 2* **1978**, *74*, 560.
(32) Doi, M.; Yamamoto, I.; Kono, F. *J. Phys. Soc. Jpn.* **1984**, *53*, 3000.
(33) Teraoka, I.; Mori, Y.; Ookubo, N.; Hayakawa, R. *Rep. Prog. Polym. Phys. Jpn.* **1984**, *27*, 127.
(34) Maguire, J. F. *J. Chem. Soc., Faraday Trans. 2* **1981**, *77*, 513.
(35) Soda, K. *J. Phys. Soc. Jpn.* **1973**, *35*, 866.
(36) Kubota, K.; Chu, B.; Fan, S.-F.; Dewey, M. M.; Brink, P.; Colflesh, D. E. *J. Mol. Biol.* **1983**, *166*, 329.
(37) Fujime, S., Kubota, K. *Macromolecules* **1984**, *17*, 441.

Determination of the Flory Interaction Parameters in Miscible Polymer Blends by Measurement of the Apparent Radius of Gyration

Alain Lapp,† Claude Picot,* and Henri Benoit

Institut Charles Sadron (CRM-EAHP), CNRS-ULP Strasbourg, 67083 Strasbourg-Cedex, France.

Received March 27, 1985

ABSTRACT: It is shown that measurement by small-angle neutron scattering of the apparent radius of gyration of a blend of two polymers having sufficient scattering contrast allows determination of the interaction parameter χ with good precision. The influence of the polydispersity of the blend components has been examined. An implementation of this method is presented with poly(dimethylsiloxane) (H and D), for which χ is far from negligible ($\chi = 1.7 \times 10^{-3}$).

The interaction parameter χ in a polymer mixture is related to the thermodynamical interaction between chains of different natures. The traditional methods used for its determination have been therefore of a thermodynamical nature: cloud point determination, heat of mixing, or zero-angle scattering. In all these approaches the Flory–Huggins expression for the free energy of mixing has been

† On leave from Laboratoire Léon Brillouin, CEN Saclay, 91191 Gif-sur-Yvette, France.

0024-9297/85/2218-2437$01.50/0